Inorganic Chemistry

ARTICLE

pubs.acs.org/IC

Structural, Electronic, and Acid/Base Properties of $[Ru(bpy)_2(bpy(OH)_2)]^{2+}$ (bpy = 2,2′-Bipyridine, $bpy(OH)_2$ = 4,4′-Dihydroxy-2,2′-bipyridine)

Samantha Klein, William G. Dougherty, W. Scott Kassel, Timothy J. Dudley, and Jared J. Paul*

Department of Chemistry, Villanova University, Villanova, Pennsylvania 19085, United States

Supporting Information

ABSTRACT: We have synthesized the complex $[Ru(bpy)_2(bpy(OH)_2)]^{2+}$ (bpy =2,2′-bipyridine, $bpy(OH)_2$ = 4,4′-dihydroxy-2,2′-bipyridine). Experimental results coupled with computational studies were utilized to investigate the structural and electronic properties of the complex, with particular attention paid toward the effects of deprotonation on these properties. The most distinguishing feature observed in the X-ray structural data is a shortening of the CO bond lengths in the modified ligand upon deprotonation. Similar results are also observed in the computational studies as the CO bond becomes double bond in character after deprotonating the complex. Electrochemically, the hydroxy-modified bipyridyl ligand plays a significant role in the redox properties of the complex. When protonated, the $bpy(OH)_2$ ligand undergoes irreversible reduction processes; however, when deprotonated, reduction of the substituted ligand is no longer observed, and several new irreversible oxidation processes associated with the modified ligand arise. pH studies indicate $[Ru(bpy)_2(bpy(OH)_2)]^{2+}$ has two distinct deprotonations at pK_{a1} = 2.7 and pK_{a2} = 5.8. The protonated $[Ru(bpy)_2(bpy(OH)_2)]^{2+}$ complex has a characteristic UV/Visible absorption spectrum similar to the well-studied complex $[Ru(bpy)_3]^{2+}$ with bands arising from Metal-to-Ligand Charge Transfer (MLCT) transitions. When the complex is deprotonated, the absorption spectrum is altered significantly and becomes heavily solvent dependent. Computational methods indicate that the deprotonated $bpy(O^-)_2$ ligand mixes heavily with the metal d orbitals leading to a new absorption manifold. The transitions in the complex have been assigned as mixed Metal−Ligand to Ligand Charge Transfer (MLLCT).

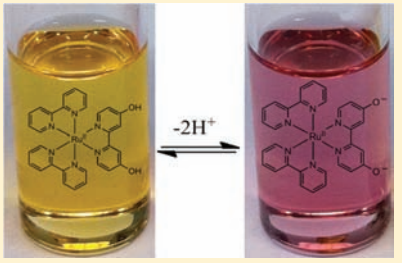

INTRODUCTION

Electron transfer is often found coupled to proton transfer reactions in both biological and chemical systems. Some of the most fundamental chemical reactions of interest, including water oxidation, nitrogen fixation, and the reduction of carbon dioxide to useful fuels, require the transfer of multiple reductive equivalents along with multiple protons, eqs 1−3.

$$2H_2O \rightarrow O_2 + 4H^+ + 4e^- \quad (1)$$

$$N_2 + 8H^+ + 8e^- \rightarrow 2NH_3 + H_2 \quad (2)$$

$$CO_2 + 4H^+ + 8e^- \rightarrow CH_4 + O_2 \quad (3)$$

In many redox active proteins, such as cytochrome c oxidase and photosystem II, the transfer of electrons is intricately connected to a proton pumping mechanism that establishes a proton gradient across a membrane necessary for energy production.[1−3] In other systems, such as tyrosine oxidation in photosystem II, the coupling of proton transfer to electron transfer provides an energetically favorable pathway that otherwise would render the protein inactive under physiological conditions.[3,4]

As a result of the common coupling of proton transfer events to electron transfer, many chemists have investigated the fundamental aspects of coupled electron−proton transfer.[5−12] Hammarström, and in collaboration with Nocera, has synthesized metal complexes with ligands containing phenol groups to study mechanistics of proton coupled electron transfer.[13−15] Phenol-substituted bipyridines have also been utilized to study the electronic properties of bimetallic complexes with bipyridine coordinated to ruthenium and the phenoxide bound to another metal, such as tungsten.[16] Meyer et al have used $Os(bpy)_3^{2+}$ (bpy =2,2′-bipyridine) to study the oxidation of the tyrosine phenol in the presence of phosphate base.[17,18] Most of the studies are mechanistic, focusing on how the proton and electron transfer occurs. Studies have also been carried out on metal complexes with hydroxy-modified polypyridyl ligands, demonstrating acid/base tunability for the reduction of carbon dioxide to formic acid.[19,20] In these systems, the deprotonated form of the catalyst is active toward carbon dioxide reduction, but as the formic acid builds up, the complex is protonated and the catalyst becomes inactive.[20] There have been few studies on the structural and electronic properties of the metal complexes with hydroxy-modified polypyridyl ligands and the effects of deprotonation.[21−24]

We are interested in the study of metal polypyridyl complexes with simple ligand structures that will greatly influence the electronic properties of the complex depending upon the

Received: August 21, 2010
Published: February 28, 2011

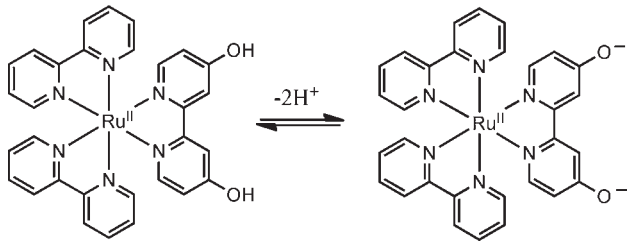

Figure 1. Depiction of $[Ru(bpy)_2(bpy(OH)_2)]^{2+}$ and the deprotonated form, $[Ru(bpy)_2(bpy(O^-)_2)]$.

protonation state of the ligand. Recently, there has been an increased interest in catalysts with properties that can be tuned with ligand protonation state.[25,26] We report here the synthesis and the structural and electronic characterization of $[Ru(bpy)_2(bpy(OH)_2)]^{2+}$ (bpy =2,2′-bipyridine; $bpy(OH)_2$ = 4,4′-dihydroxy-2,2′-bipyridine), Figure 1. The $bpy(OH)_2$ ligand contains two hydroxyl groups that can be readily deprotonated. The crystal structures of the protonated and deprotonated forms of the complex are compared to structures determined computationally in the gas phase as well as two different solvents, water and 1,2-dichloroethane. The protonation state of the $bpy(OH)_2$ ligand greatly alters the absorbance properties of the complex, and these effects are highly solvent dependent. Recent work on ruthenium terpyridine complexes has demonstrated that computational methods in concert with experimental studies can be utilized to gain an understanding of the electronic properties of the complexes and the role of the solvent.[27] Therefore, we investigated the origin of the visible charge transfer bands in both the protonated and the deprotonated $[Ru(bpy)_2(bpy(OH)_2)]^{2+}$ complex by computational methods. As a basis for comparison, the control complexes $[Ru(bpy)_3]^{2+}$ and $[Ru(bpy)_2(bpy(OMe)_2)]^{2+}$ ($bpy(OMe)_2$ = 4,4′-dimethoxy-2,2′-bipyridine) were studied experimentally and computationally. The $bpy(OMe)_2$ ligand has similar properties when compared to the $bpy(OH)_2$ ligand, with the exception that the methoxy group does not have the ability to be deprotonated and therefore, the electronic properties do not change as a function of acid and base.

EXPERIMENTAL SECTION

General Procedures. Reagents were obtained from Aldrich Chemical Co. and used without further purification. $RuCl_3 \cdot 3H_2O$ was purchased from Pressure Chemical Co. $Ru(bpy)_2Cl_2$ and 4,4′-dihydroxy-2,2′-bipyridine were synthesized using previously reported procedures.[28,29] $[Ru(bpy)_3][Cl]_2$ was prepared according to a previously published method and converted to the hexafluorophosphate salt by metathesis.[30] Elemental analyses for ruthenium complexes were carried out by Atlantic Microlab Inc., Norcross, GA. For studies done in aqueous solutions, all ruthenium hexfluorophosphate salts were converted to chloride salts by precipitation from acetone using tetrabutylammonium chloride dissolved in acetone. Aqueous solutions were prepared using a Millipore DirectQ UV water purification system.

^{1}H NMR spectra were collected on a Varian 300 MHz Fourier Transform spectrometer in deuterated acetonitrile (CD_3CN). UV−visible absorption spectra were collected on a Scinco S-3100 diode-array spectrophotometer at a resolution of 1 nm. pH measurements were performed using a VWR SympHony pH meter, utilizing a three point calibration at pH = 4, 7, and 10.

Electrochemical measurements were carried out on a Bioanalytical Systems (BAS) CW-50 potentiostat. A standard three electrode setup with a Ag/Ag^+ reference electrode, platinum wire auxiliary electrode, and glassy carbon working electrode was used. All measurements were taken in 0.1 M tetrabutylammonium hexafluorophosphate ($TBAPF_6$) in acetonitrile electrolyte solution. The solutions were degassed for approximately 15 to 20 min with argon before data collection. Ferrocene was used as an internal standard with $E_{1/2}$ = +0.40 V vs SCE.[31]

Synthesis. *$[Ru(bpy)_2(bpy(OMe)_2)][PF_6]_2$.* A round-bottom flask containing 30 mL of ethylene glycol was degassed with argon for 30 min. A 0.5311 g (1.096 mmol) sample of $Ru(bpy)_2(Cl)_2$ was added to the reaction flask and heated to 155 °C for 3 h. To the flask, 0.3303 g of (1.528 mmol) of 4,4′-dimethoxy-2,2′-bipyridine was added and heating was continued for 3 h. After the reaction was completed, the solution was cooled to room temperature. To the solution, an excess solution of NH_4PF_6 in 20 mL of water was added to precipitate the orange-red complex. The complex was filtered and washed with ether. For purification, the complex was dissolved in acetone, filtered, and precipitated as the chloride salt using tetrabutylammonium chloride (TBACl) followed by rinsing with acetone. The complex was dissolved in water, precipitated using NH_4PF_6, and rinsed with water, followed by ether. Yield: 0.77 g (0.84 mmol), 77%. ^{1}H NMR (300 MHz, CD_3CN): δ 8.5 (dd, 4H), 8.0 (m, 6H), 7.8 (d, 2H), 7.7 (d, 2H), 7.4 (m, 6H), 6.9 (dd, 2H), 4.0 (s, 6H). Anal. Calcd for $RuC_{32}N_6O_2H_{28}P_2F_{12}$: C, 41.80; N, 9.14; H, 3.07%. Found: C, 41.69; N, 9.06; H, 2.94%.

$[Ru(bpy)_2(bpy(OH)_2)][PF_6]_2$. A round-bottom flask containing 30 mL of a 1:1 ethanol/water mixture was degassed with argon for 30 min. A 0.4661 g (0.9623 mmol) sample of $Ru(bpy)_2(Cl)_2$ and a 0.2190 g (1.164 mmol) sample of 4,4′-dihydroxy-2,2′-bipyridine were added to the flask and heated at 80 °C for 3 h under argon. After the reaction was completed, the solution was allowed to cool to room temperature and filtered to remove any insoluble unreacted ligand. A 10-fold molar excess NH_4PF_6 in 100 mL of water was added to precipitate the complex. The complex was filtered and rinsed with water followed by ether. For purification, the complex was dissolved in acetone, filtered, and precipitated as the chloride salt using tetrabutylammonium chloride (TBACl) followed by rinsing with acetone. The complex was dissolved in water and a few drops of concentrated hydrochloric acid were added to ensure protonation of the ligand hydroxyl groups. The solution was precipitated using NH_4PF_6, filtered and rinsed with water, then ether. Yield: 0.2124 g (0.2382 mmol), 25%. ^{1}H NMR (300 MHz, CD_3CN): δ 8.5 (m, 4H), 8.0 (m, 4H), 7.85 (d, 2H), 7.8 (d, 2H), 7.7 (d, 2H), 7.4 (m, 6H), 6.85 (dd, 2H). Anal. Calcd for $RuC_{30}N_6O_2H_{24}P_2F_{12} \cdot H_2O$: C, 39.62; N, 9.24; H, 2.88%. Found: C, 40.02; N, 8.94; H, 3.11%.

X-ray Structural Analysis. *$[Ru(bpy)_2(bpy(OH)_2)]^{2+}$.* Crystals of $[Ru(bpy)_2(bpy(OH)_2)]^{2+}$ were grown by the slow diffusion of ether into a benzonitrile solution of the dissolved complex. A single red plate (0.04 × 0.24 × 0.27 mm) was mounted using NVH immersion oil onto a nylon fiber and cooled to the data collection temperature of 100(2) K. Data were collected on a Brüker-AXS Kappa APEX II CCD diffractometer with 0.71073 Å Mo-Kα radiation. Unit cell parameters were obtained from 90 data frames, 0.3° Φ, from three different sections of the Ewald sphere yielding a = 11.835(1) Å, b = 28.306(2) Å, c = 14.716(1) Å, β = 93.195(2)°, V = 4922(1) Å^3. A total of 65664 reflections (R_{int} = 0.0361) were collected (18801 unique) over q = 1.56 to 33.21°. The systematic absences in the diffraction data were consistent with the centrosymmetric, monoclinic space group, $P2_1/n$. The data set was treated with SADABS absorption corrections based on redundant multiscan data (Sheldrick, G., Bruker-AXS, 2001) T_{max}/T_{min} = 1.11. The asymmetric unit contained one $[Ru(bpy)_2(bpy(OH)_2)]^{2+}$ cation, two $[PF_6]^-$ anions, two molecules of benzonitrile, and one molecule of diethyl ether all located on general positions yielding a Z = 4 and a Z' = 1. One of the anions is disordered over two positions, which were located from the difference map and restrained using SAME and EADP commands to stabilize the refinement. The other $[PF_6]^-$ anion is likely disordered based on the thermal parameters, but the refinement of this disorder would not stabilize, so it was ignored. All non-hydrogen

dx.doi.org/10.1021/ic1017054 |Inorg. Chem. 2011, 50, 2754–2763

Table 1. Selected Bond Lengths (Å) and Bond Angles (deg) for Ruthenium Complexes

$[Ru(bpy)_2(bpy(OH)_2)]^{2+}$		$[Ru(bpy)_2(bpy(O^-)_2)]$	
Bond Lengths			
Ru(1)−N(1)	2.0611(18)	Ru(1)−N(1)	2.068(2)
Ru(1)−N(2)	2.058(2)	Ru(1)−N(2)	2.066(2)
Ru(1)−N(3)	2.061(2)	Ru(1)−N(3)	2.051(2)
Ru(1)−N(4)	2.0590(19)	Ru(1)−N(4)	2.044(2)
Ru(1)−N(5)	2.059(2)	Ru(1)−N(5)	2.057(2)
Ru(1)−N(6)	2.059(2)	Ru(1)−N(6)	2.048(2)
C(3)−O(1)	1.342(3)	C(3)−O(1)	1.283(3)
C(8)−O(2)	1.335(3)	C(8)−O(2)	1.294(3)
Bond Angles			
N(1)−Ru(1)−N(2)	78.50(8)	N(1)−Ru(1)−N(2)	78.52(8)
N(1)−Ru(1)−N(3)	96.15(8)	N(1)−Ru(1)−N(3)	94.47(9)
N(1)−Ru(1)−N(4)	171.86(8)	N(1)−Ru(1)−N(4)	170.42(8)
N(1)−Ru(1)−N(5)	89.84(8)	N(1)−Ru(1)−N(5)	87.92(8)
N(1)−Ru(1)−N(6)	95.70(8)	N(1)−Ru(1)−N(6)	97.51(8)

atoms were refined with anisotropic displacement parameters. All hydrogen atoms were treated as idealized contributions. The goodness of fit on F^2 was 1.029 with $R1(wR2)$ 0.0535(0.1185) for $[Iq > 2(I)]$ and with largest difference peak and hole of 1.319 and −1.117 e/Å^3 because of a small amount of unresolved disorder in one of the $[PF_6]^-$ anions.

[Ru(bpy)$_2$(bpy(O$^-$)$_2$)]. Crystals of $[Ru(bpy)_2(bpy(O^-)_2)]$ were grown by precipitation from an acetonitrile solution of $[Ru(bpy)_2(bpy(OH)_2)]^{2+}$ with aqueous tetrabutylammonium hydroxide. A single red block (0.10 × 0.10 × 0.13 mm) was mounted using NVH immersion oil onto a glass fiber and cooled to the data collection temperature of 100(2) K. Data were collected on a Brüker-AXS Kappa APEX II CCD diffractometer with 0.71073 Å Mo-Ka radiation. Unit cell parameters were obtained from 90 data frames, 0.3° Φ, from three different sections of the Ewald sphere yielding a = 23.391(2) Å, b = 13.355(2) Å, c = 20.589(2) Å, β = 99.200(4)°, V = 6349(1) Å^3. A total of 74556 reflections were collected (23825 unique, R_{int} = 0.0805) over q = 1.76 to 33.13°. The systematic absences in the diffraction data were consistent with the centrosymmetric, monoclinic space group, $P2_1/c$. The data set was treated with SADABS absorption corrections based on redundant multiscan data (Sheldrick, G., Bruker-AXS, 2001) T_{max}/T_{min} = 1.02. The asymmetric unit contains two independent RuL_3 molecules, two acetonitrile solvent molecules, and 9 solvent water molecules. The solvent was located from the difference map and allowed to refine freely. The protons on the water molecules were located from the difference map except in two cases where they would not survive refinement. Those four protons were left out of the structure, but the chemical formula modified to include them. There is a residual Q-peak remaining above 2.656, that looks like another water molecule but even at half occupancy it does not refine well as an oxygen atom. It was modeled as it is in free space and has no bearing on the identity of the parent molecule. All molecules were located on general positions yielding Z = 4, and Z' = 2. All non-hydrogen atoms were refined with anisotropic displacement parameters. All other hydrogen atoms were treated as idealized contributions. The goodness of fit on F^2 was 1.022 with $R1(wR2)$ 0.0509(0.1021) for $[Iq > 2(I)]$ and with largest difference peak and hole of 2.656 and −0.931 e/Å^3.

Computational Methods. All calculations were performed using GAMESS.[32] Geometries were optimized using B3LYP with the 6-31G* basis set for main group elements and a scalar relativistic Huzinaga model core potential[33,34] (MCP) for ruthenium. The default grid size was used for numerical integration in density functional theory (DFT) calculations. Spherical harmonic d-orbitals were used in all calculations. The maximum tolerance for nuclear gradients was set to 0.001 hartree/bohr. The nature of each minimum was determined by running analytic frequencies at RHF optimized structures. The RHF geometries did not differ drastically from DFT optimized geometries, and all structures were found to have zero imaginary frequencies. Vertical excitation energies were calculated using time-dependent DFT (TDDFT) with the same set of functionals and basis sets used in the ground state calculations. Solvent effects on the vertical excitation energies were evaluated using the PCM solvation model. The solute cavity was determined using the simplified united atomic radii implemented in GAMESS. The two solvents considered in this work were water and 1,2-dichloroethane.

RESULTS AND DISCUSSION

Structural Characterization. The $[Ru(bpy)_2(bpy(OH)_2)]^{2+}$ complex was structurally characterized by X-ray diffraction and computational methods. Select bond lengths and angles are reported in Table 1 and the corresponding structure is depicted in Figure 2a. The Ru center is a distorted octahedral shape with adjacent N−Ru−N bond angles ranging from 78.50(8)° to 98.16(8)°. This distorted octahedral shape is similar to the parent, $[Ru(bpy)_3]^{2+}$ complex, with adjacent N−Ru−N bond angles ranging from 78.65° to 96.30°.[35] Ru−N bond lengths of the hydroxylated complex range from 2.058(2) Å to 2.061(2) Å, also similar to the parent $[Ru(bpy)_3]^{2+}$ complex.

The crystal structure of the hydroxylated complex has many similarities in bond lengths and angles compared to the methoxy-substituted complex, $Ru(bpy)_2(bpy(OMe)_2)]^{2+}$.[36] The C−O bond lengths in the hydroxylated complex (1.342(3) Å and 1.335(3) Å) are analogous to the methoxy complex (1.345 Å and 1.342 Å). These bond lengths are consistent with the electron-donating nature of the hydroxy and methoxy groups. Crystals of the fully deprotonated complex $[Ru(bpy)_2(bpy(O^-)_2)]$ were also grown, and relevant bond lengths and angles are reported in Table 1 with the corresponding structure depicted in Figure 2b. There is not a significant change in the bond lengths or angles in the crystal structure upon deprotonation with the exception of the shortening of the C−O bond lengths from 1.342(3) Å and 1.335(3) Å to 1.283(3) Å and 1.294(3) Å respectively. The observed shortening of the C−O bonds is readily explained by the resonance structures that are possible upon deprotonation, Figure 3.

Computational studies have been carried out on the ground state bis-protonated $[Ru(bpy)_2(bpy(OH)_2)]^{2+}$ complex and the completely deprotonated form of the complex, $[Ru(bpy)_2(bpy(O^-)_2)]$. The relevant bond lengths associated with both complexes in water, 1,2-dichloroethane, and in the gas phase, are reported in Table 2. The numbering system for this complex is the same as that used for the crystal structure analysis. All calculated structures are distorted octahedral complexes with Ru−N bond lengths slightly elongated compared to the crystal structure. The adjacent N−Ru−N bond angles in the gas phase calculation range from 77.71° to 96.12°, and are all within one degree of the corresponding observed bond angles in the crystal structure. The addition of solvent in the calculations does not significantly alter the bond angles within the complex. The C−O bond length of the protonated complex in the gas phase is 1.338 Å and only negligibly longer at 1.341 Å in the presence of solvent, which is similar to the corresponding bond length observed in the crystal structure. Upon deprotonation, the C−O bond length decreases significantly in the gas phase to 1.245 Å and becomes more double bond in character. In the presence of both water and

dx.doi.org/10.1021/ic1017054 |*Inorg. Chem.* 2011, 50, 2754–2763

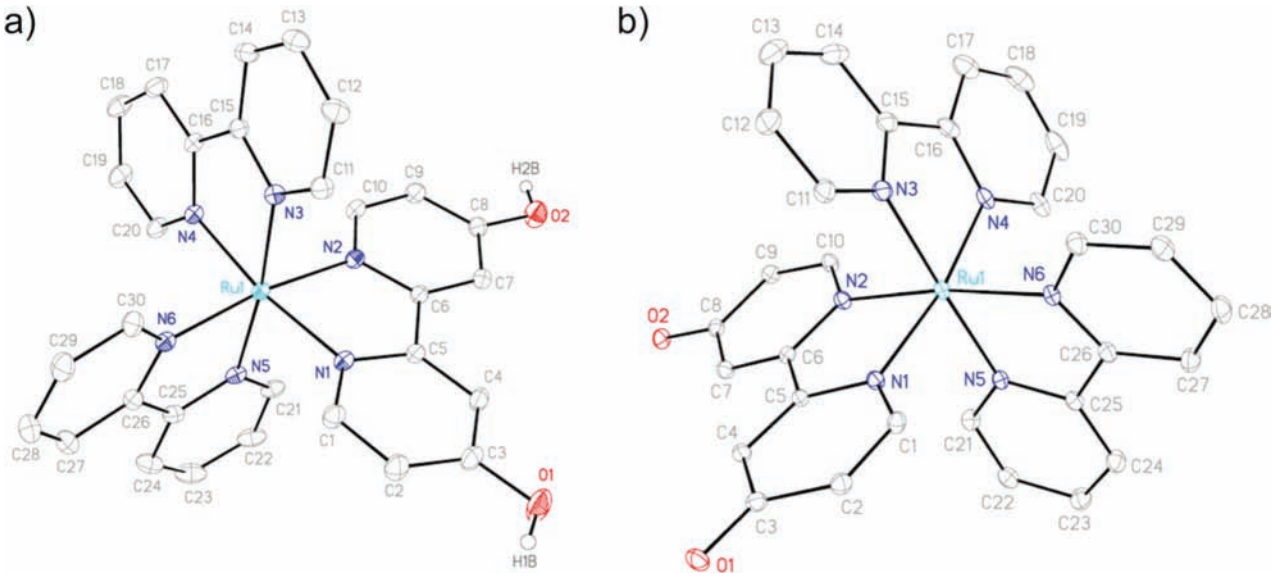

Figure 2. Crystal structures of (a) $[Ru(bpy)_2(bpy(OH)_2]^{2+}$ and (b) $[Ru(bpy)_2(bpy(O^-)_2)]$.

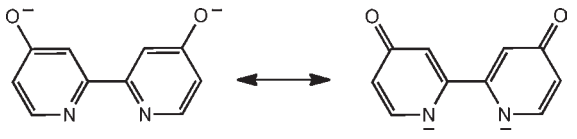

Figure 3. Resonance structures of deprotonated $bpy(O^-)_2$ ligand.

1,2-dichloroethane solvent, the average bond lengths are longer (1.261 Å) than calculated in the gas phase. These bond lengths are shorter than the C−O bond lengths of 1.283(3) Å and 1.294(3) Å observed in the crystal structure. However, the crystal structure of the completely deprotonated complex has a significant number of solvent specific water molecule interactions that can hydrogen bond with the deprotonated oxygen atoms in the complex, thus lengthening the actual observed C−O bond.

Computational studies were also performed on $[Ru(bpy)_3]^{2+}$ and $[Ru(bpy)_2(bpy(OMe)_2)]^{2+}$ to provide a complete comparison of all complexes. Nuclear coordinates are reported in the Supporting Information. Both complexes adhere to the distorted octahedral shape observed in all previous complexes with adjacent N−Ru−N bond angles ranging from 77.58° to 97.19°. All of the Ru−N bond lengths are comparable to the protonated complex with bond lengths ranging from 2.105 Å to 2.107 Å for $[Ru(bpy)_3]^{2+}$ and 2.095 Å to 2.104 Å for $[Ru(bpy)_2(bpy(OMe)_2)]^{2+}$. In addition, the C−O bond length in the methoxy-modified complex has a calculated bond length of 1.333 Å, which is similar to the hydroxy-modified complex. As a result of these observations, we conclude that structurally, the hydroxy-modified complex is very similar in structure to the corresponding methoxy-modified complex. Upon deprotonation, however, there is a significant change in the structure, which is reflected in the electronic absorbance spectroscopy, vide infra.

Electrochemistry. Cyclic voltammetry measurements on all three ruthenium complexes gave reversible waves from the $Ru^{III/II}$ couple. The complex $[Ru(bpy)_2(bpy(OH)_2)]^{2+}$ gave the lowest potential at 1.16 V vs SCE, followed by $[Ru(bpy)_2(bpy(OMe)_2)]^{2+}$ at 1.18 V vs SCE. As expected, these potentials were significantly lower than the observed redox potential of $[Ru(bpy)_3]^{2+}$ with the reversible $Ru^{III/II}$ couple at 1.30 V vs SCE. The hydroxy- and methoxy- substituted groups are electron-donating and stabilize the Ru^{III} oxidation state compared to the unsubstituted bipyridine complex resulting in the observed redox potential trend. By way of further illustration, $[Ru(bpy(OMe)_2)_3]^{2+}$, which has three methoxy-substituted bpy ligands, has been found to have a reduction potential of 0.85 V vs SCE because of the increasing electron-donating nature of the substituted $bpy(OMe)_2$ ligand.[37]

The $[Ru(bpy)_3]^{2+}$ and $[Ru(bpy)_2(bpy(OMe)_2)]^{2+}$ complexes both have reversible waves from the bipyridine ligands. For $[Ru(bpy)_3]^{2+}$, the waves were observed at −1.33 V, −1.53 V, and −1.79 V vs SCE while for $[Ru(bpy)_2(bpy(OMe)_2)]^{2+}$, the waves occurred at −1.37 V, −1.58 V, and −1.81 V vs SCE. Cyclic voltammograms of $[Ru(bpy)_3]^{2+}$ and $[Ru(bpy)_2(bpy(OMe)_2)]^{2+}$ are available in the Supporting Information. $[Ru(bpy)_2(bpy(OH)_2)]^{2+}$ yielded several reduction waves in the range from −1.40 to −1.85 V in addition to the appearance of two oxidation waves in this region, Figure 4. However, these waves could not be distinguished because of heavy overlap and a significant degree of irreversibility. Also, during a complete scan, after reducing and reoxidizing the bipyridine ligands in $[Ru(bpy)_2(bpy(OH)_2)]^{2+}$, another new oxidation wave appears at 0.78 V vs SCE. This oxidation wave is not observed when scanning between 0 and 1.80 V. Clearly, the addition of the $bpy(OH)_2$ ligand on the complex is the source of this irreversibility.

The electrochemistry of $[Ru(bpy)_2(bpy(OH)_2)]^{2+}$ changes significantly upon deprotonation, Figure 4. Cyclic voltammograms of $[Ru(bpy)_2(bpy(O^-)_2)]$ were collected by using tetrabutylammonium hydroxide to deprotonate the complex. Two reversible redox waves appear at −1.55 and −1.81 V vs SCE that are attributed to reduction of the unmodified bipyridine ligands. These redox waves are comparable to the second and third bipyridine redox waves observed in the $[Ru(bpy)_3]^{2+}$ and $[Ru(bpy)_2(bpy(OMe)_2)]^{2+}$ complexes. There are several new irreversible oxidations that appear at potentials above 0 V vs SCE. The two lowest oxidation waves occur at 0.27 and 0.55 V vs SCE. Upon deprotonation, phenols have significantly lower oxidation potentials, most notably observed in the oxidation of tyrosine as a function of pH.[38] Although each of the current peaks were not

dx.doi.org/10.1021/ic1017054 |*Inorg. Chem.* 2011, 50, 2754–2763

Table 2. Calculated Bond Lengths (Å) and Bond Angles (deg) for $[Ru(bpy)_2(bpy(OH)_2)]^{2+}$

solvent	gas	gas	water	water	DCE	DCE
protonation state	$bpy(OH)_2$	$bpy(O^-)_2$	$bpy(OH)_2$	$bpy(O^-)_2$	$bpy(OH)_2$	$bpy(O^-)_2$
			Bond Lengths			
Ru(1)−N(1)	2.109	2.070	2.099	2.090	2.101	2.092
Ru(1)−N(2)	2.109	2.070	2.098	2.090	2.099	2.091
Ru(1)−N(3)	2.100	2.069	2.090	2.079	2.091	2.080
Ru(1)−N(4)	2.100	2.110	2.092	2.103	2.093	2.102
Ru(1)−N(5)	2.100	2.069	2.093	2.079	2.093	2.079
Ru(1)−N(6)	2.100	2.110	2.093	2.104	2.093	2.103
C(3)−O(1)	1.338	1.245	1.342	1.262	1.341	1.261
C(8)−O(2)	1.338	1.245	1.341	1.261	1.341	1.260
			Bond Angles			
N(1)−Ru(1)−N(2)	77.71	78.53	77.87	77.94	77.85	77.94
N(1)−Ru(1)−N(3)	96.09	94.75	96.23	95.38	96.15	95.52
N(1)−Ru(1)−N(4)	171.66	171.15	172.20	171.67	172.03	171.84
N(1)−Ru(1)−N(5)	89.87	91.98	89.15	91.22	89.53	90.94
N(1)−Ru(1)−N(6)	96.12	96.31	96.23	96.56	96.10	96.58

assigned as metal-centered, ligand-centered, or mixed metal-ligand centered oxidations, computational studies were performed to help understand the structure of the filled molecular orbitals of the complex, vide infra.

Cyclic voltammetry data was also obtained for the monodeprotonated, $[Ru(bpy)_2(bpy(OH)(O^-))]^+$, which was made by the addition of one stoichiometric equivalent of tetrabutylammonium hydroxide, Figure 4. The voltammogram clearly shares features of both the fully protonated and fully deprotonated forms of the complex. The monodeprotonated complex has reversible waves at −1.53 and −1.80 V vs SCE that are similar in potential to the reversible bpy waves observed in the deprotonated complex. There is also an irreversible reductive wave at −1.77 V vs SCE that matches the sharp reductive wave at −1.77 V vs SCE observed in the fully protonated complex. The monodeprotonated complex has a significant number of oxidation waves above 0 V vs SCE. Most notably, the first irreversible oxidation wave occurs at 0.57 V vs SCE, similar to the second oxidation wave in the completely deprotonated complex (0.55 V vs SCE). It is not surprising that the completely deprotonated complex has the overall lowest energy oxidation (0.27 V vs SCE) as significant negative charge has built up on the modified $bpy(O^-)_2$ ligand.

Absorbance Spectroscopy. UV/Visible absorption data was collected for $[Ru(bpy)_2(bpy(OH)_2)]^{2+}$ in water, Figure 5. Table 3 gives peak maxima and the molar absorptivities of these peaks. The observed absorbance bands were very similar to those seen for $[Ru(bpy)_3]^{2+}$ and $[Ru(bpy)_2(bpy(OMe)_2)]^{2+}$ in water (Supporting Information).[39] There are several intense transitions in the wavelength range from 240 to 300 nm that are assigned to $\pi-\pi^*$ transitions.[40] The electronic transitions that appear at wavelengths higher than 300 nm in $[Ru(bpy)_3]^{2+}$ are the result of many overlapping MLCT bands from the metal-centered d orbitals to the ligand π^* orbitals and are therefore assigned similarly for $[Ru(bpy)_2(bpy(OH)_2)]^{2+}$.[41] The lowest energy MLCT transition observed for $[Ru(bpy)_2(bpy(OH)_2)]^{2+}$ occurs at λ_{max} = 462 nm, similar to the corresponding MLCT transition in $[Ru(bpy)_2(bpy(OMe)_2)]^{2+}$ (λ_{max} = 461 nm) and red-shifted compared to the MLCT transition in $[Ru(bpy)_3]^{2+}$ (λ_{max} = 451 nm) in water. These wavelength shifts scale with the electron-donating ability of the ligands, which leads to a destabilization of the filled d-orbitals, resulting in lower transition energies. In addition, these results follow the same trend observed for the $Ru^{III/II}$ redox potential as a function of ligand, vide supra.

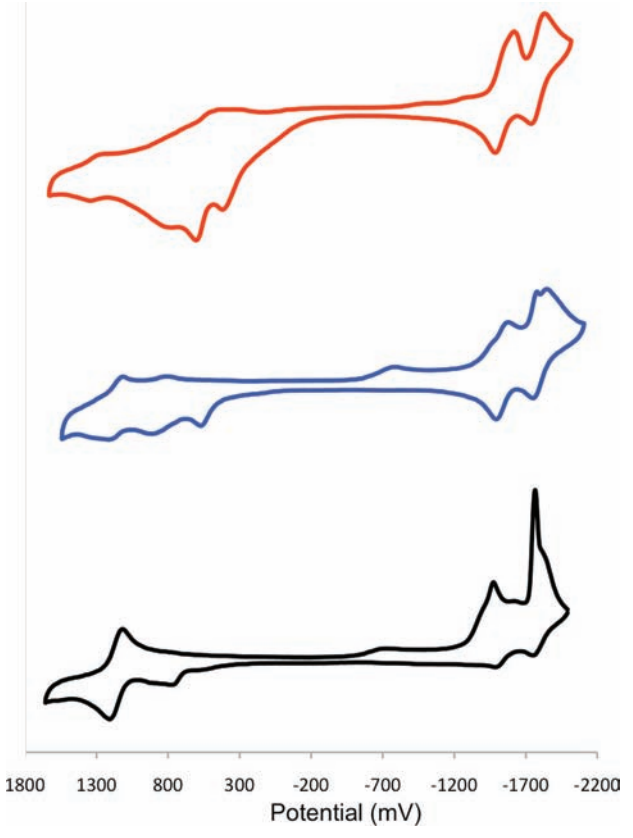

Figure 4. Cyclic Voltammogram of (black line) $[Ru(bpy)_2(bpy(OH)_2)]^{2+}$, (blue line) $[Ru(bpy)_2(bpy(OH)(O^-))]^+$, and (red line) $[Ru(bpy)_2(bpy(O^-)_2)]$ in acetonitrile with 0.1 M tetrabutylammonium hexafluorophosphate. Data reported versus SCE.

dx.doi.org/10.1021/ic1017054 |*Inorg. Chem.* 2011, 50, 2754–2763

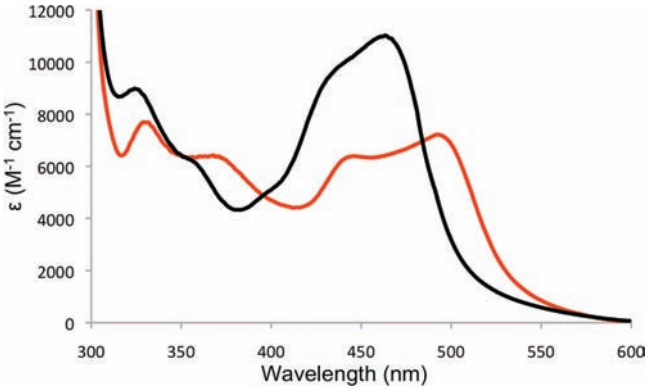

Figure 5. UV/Visible spectrum of (black line) $[Ru(bpy)_2(bpy(OH)_2)]^{2+}$ and (red line) $[Ru(bpy)_2(bpy(O^-)_2)]$ in water.

Table 3. UV/Visible Absorption Data for $[Ru(bpy)_2(bpy(OH)_2)][Cl]_2$ in Water

complex	energy (eV)	λ (nm)	ε (M^{-1} cm^{-1})
protonated with HCl	5.046	246(sh)	23100
	4.868	255	24400
	4.325	287	55500
	3.819	325	8980
	3.477	357(sh)	6190
	2.853	435(sh)	9670
	2.687	462	11000
deprotonated with NaOH	5.129	242	37700
	4.265	291	50300
	3.761	330	7730
	3.373	368	6460
	2.796	444	6440
	2.518	493	7280

Upon deprotonation of $[Ru(bpy)_2(bpy(OH)_2)]^{2+}$ with NaOH in aqueous solution to make $[Ru(bpy)_2(bpy(O^-)_2)]$, the spectral region between 300 and 600 nm changes significantly, Figure 5. The MLCT transitions shift from 325 and 357 nm to 330 and 368 nm, respectively. The MLCT absorption band at 462 nm forms two clearly defined absorption peak maxima at λ_{max} = 444 nm and λ_{max} = 493 nm. The $[Ru(bpy)_3]^{2+}$ and $[Ru(bpy)_2(bpy(OMe)_2)]^{2+}$ complexes absorbance spectra are not altered in either acidic or basic solution (Supporting Information). It is therefore clear that the protonation state is the cause of the electronic changes that occur with the $[Ru(bpy)_2(bpy(OH)_2)]^{2+}$ complex. Deprotonation of the $bpy(OH)_2$ ligand makes the ligand a better π-donor as depicted in Figure 3, which leads to further destabilization of the filled d orbitals. The destabilization leads to lower energy transitions for some of the MLCT bands. The lowest energy transition shift of 1300 cm^{-1} upon deprotonation is comparable to the 1500 cm^{-1} energy change that is observed in the deprotonation of $[Ru(bpy)_2(phen(OH)_2))]^{2+}$ ($phen(OH)_2$ = 4,4′-dihyroxy-1,10-phenanthroline).[21] Both of these complexes have the hydroxyl group directly attached to the bipyridine. Interestingly, $[Ru(bpy)_2(bpy(PhOH))]^{2+}$ (bpy(PhOH) = 4-(4-hydroxyphenyl)-2,2′-bipyridine), a similar complex containing a phenol attached to the bipyridine, does not undergo any wavelength shift of the lowest energy MLCT band upon deprotonation.[24] This complex

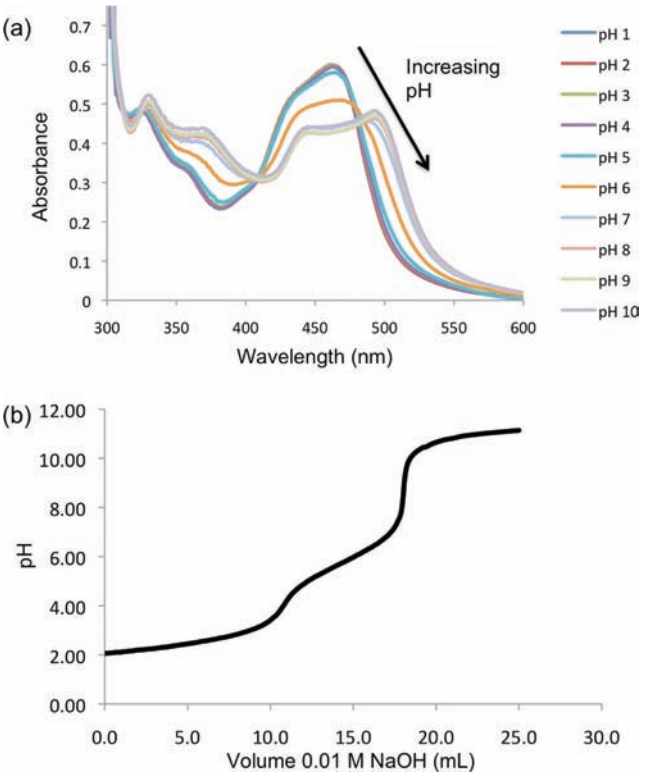

Figure 6. (a) UV/Visible spectrum of $[Ru(bpy)_2(bpy(OH)_2)]^{2+}$ in water ranging from pH = 1 to pH = 10 and (b) pH titration of $[Ru(bpy)_2(bpy(OH)_2)]^{2+}$.

does, however, give the appearance of a new absorbance band at 360 nm, which the authors ascribe to a ligand centered transition.[24] Although it is clear that the general explanation of a lower energy transition as a function of the more electron-donating ligand holds for our results, we sought to gain a better understanding of the features of the MLCT bands themselves upon deprotonation. Computational studies were utilized to help further elucidate the nature of the changes in the absorption manifold upon deprotonation, vide infra.

The absorbance spectra of $[Ru(bpy)_2(bpy(OH)_2)]^{2+}$ was collected at varying pH values to determine the pK_a of the complex, as well as to determine if two subsequent deprotonations could be observed, Figure 6a. The spectra clearly demonstrate a change beginning at pH = 5.0 to pH = 7.0 where the complex is fully deprotonated. pH titration data was collected and two pK_a values were determined with pK_{a1} = 2.7 and pK_{a2} = 5.8, Figure 6b. The values can be compared to $[Ru(phen(OH)_2)_2(bpy)]^{2+}$, a complex with four protons where the individual pK_a values could not be determined and is reported in the literature to have an average pK_a = 5.1.[37] It is clear that the first deprotonation step does not change the absorbance spectrum significantly in aqueous solution. However, during the second deprotonation step of the complex, there is a clear change in the absorption spectrum. It is unclear as to why the first deprotonation step does not result in an observed change in the electronic absorbance of the complex, although there is most likely a high degree of hydrogen bonding in the aqueous environment with the substituted ligand, which would help to explain this observation. Further studies were performed in additional solvents to determine if the result was a trend or solvent specific to water.

dx.doi.org/10.1021/ic1017054 |*Inorg. Chem.* 2011, 50, 2754–2763

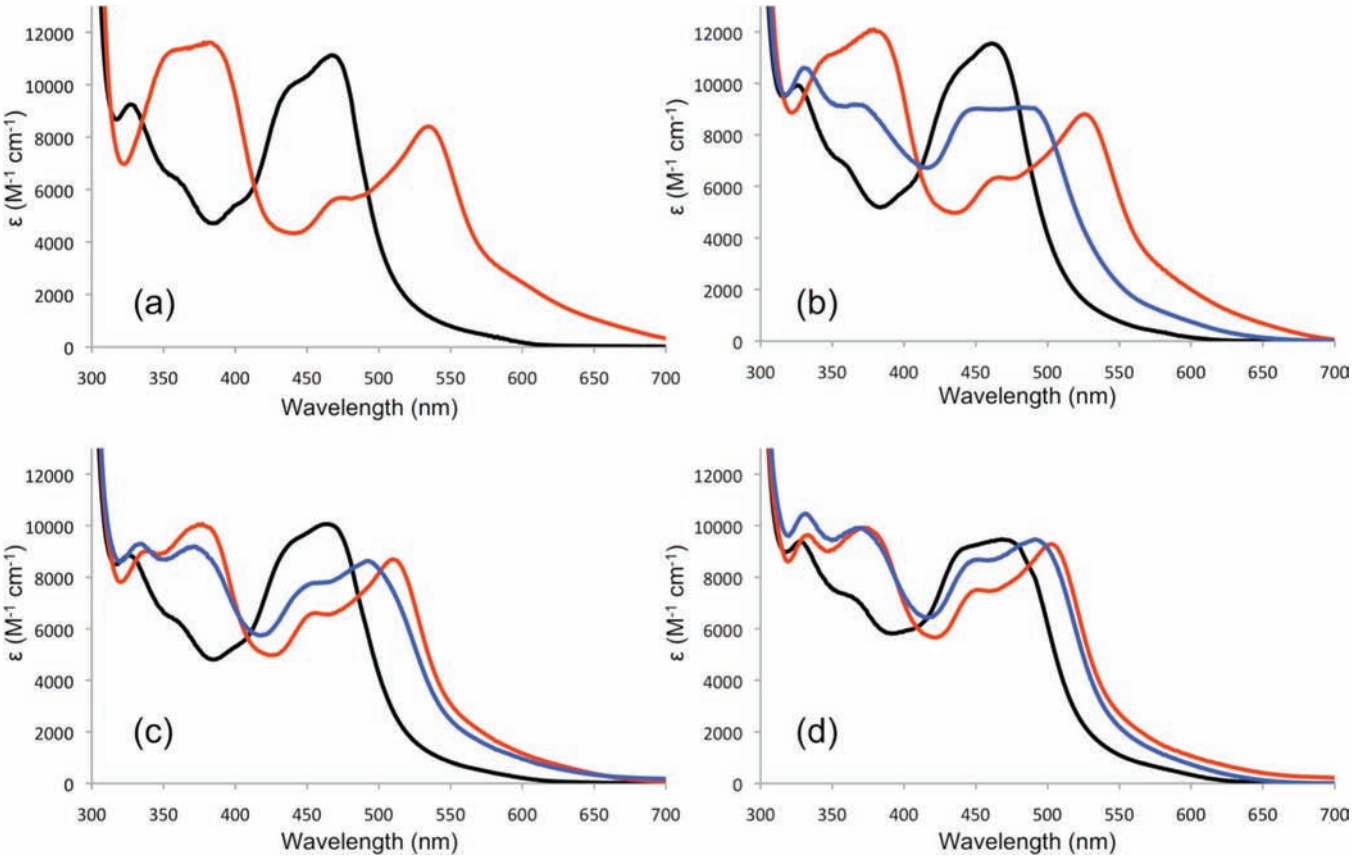

Figure 7. UV/Visible spectrum of (black lines) $[Ru(bpy)_2(bpy(OH)_2)]^{2+}$, (blue lines) $[Ru(bpy)_2(bpy(O^-)(OH))]^{+}$, and (red lines) $[Ru(bpy)_2(bpy(O^-)_2)]$ in (a) 1,2-dichloroethane, (b) acetonitrile, (c) ethanol, and (d) methanol.

Absorbance spectra of $[Ru(bpy)_2(bpy(OH)_2)]^{2+}$ were collected in four additional solvents: 1,2-dichloroethane, acetonitrile, ethanol, and methanol with the use of tetrabutylammonium hydroxide to deprotonate the complex, Figure 7. The solvents were chosen for the range in dielectric constants as well as the solvent hydrogen bonding ability. The absorbance spectrum of the protonated complex does not change significantly upon altering the solvent. The largest shift observed is of the lowest energy MLCT band that red-shifts from 462 nm (water) to 469 nm (1,2-dichloroethane). The modest lower energy shift is comparable to solvatochromatic shifts observed for $[Ru(bpy)_3]^{2+}$ upon changing the solvent from water (450 nm) to methylene chloride (453 nm).[42]

The wavelength maxima of the fully deprotonated complex in varying solvents are significantly shifted when compared to water. All of the absorbance maxima in the range from 300 to 600 nm shift to lower energy and these shifts are attributed to two factors: (1) hydrogen bonding ability of the solvent and (2) dielectric constant of the solvent. When comparing the lowest energy λ_{max} of the fully deprotonated complex in the hydrogen bonding solvents: (water, methanol, and ethanol), the energy shifts scale with the dielectric constants of the solvent. That is, the deprotonated complex shifts from 493 nm in water to 503 nm in methanol to 511 nm in ethanol. The overall shift is approximately 700 cm^{-1} in energy. Even larger shifts are observed when the non-hydrogen-bonding solvents acetonitrile and 1,2-dichloroethane were examined. The observed λ_{max} of the deprotonated complex is 526 nm in acetonitrile and 534 nm in 1,2-dichloroethane, shifting 1300 cm^{-1} and 1600 cm^{-1}, respectively, from the deprotonated form in water. Of the additional solvents studied, acetonitrile has the highest dielectric constant when compared to water. The fact that the shifts are larger in non-hydrogen bonding solvents compared to hydrogen bonding solvents experimentally supports the hypothesis that there are solvent-specific interactions between the deprotonated phenoxide of the bipyridine ring structure and hydroxyl protons in the solvent resulting in a smaller effect on the electronic structure of the complex.

Comparing the protonated form of the complex with the completely deprotonated form of the complex in all solvents provided significant changes in the absorbance spectrum. These energy shifts were all larger than those observed in water. For example, the lowest energy λ_{max} for the completely deprotonated complex was observed for 1,2-dichloroethane at 534 nm, shifted by 2600 cm^{-1} compared to the protonated form in 1,2-dichloroethane. This energy change is double the energy shift observed upon deprotonation of the complex in water (1300 cm^{-1}).

Further studies were carried out to stoichiometrically deprotonate the complex by only one proton in the varying solvents to compare the monodeprotonated form of the complex to that observed in water during the pH studies, Figure 7b−d. In all cases the monodeprotonated complex demonstrated a lower energy shift compared to the fully protonated complex in the varying solvents. This is not surprising because a single deprotonation can still result in π-donation to the metal center from one of the pyridine rings, Figure 8. Similar results were observed in 1,2-dichloroethane, but a stoichiometric monodeprotonation could not be accurately obtained because of the low solubility of

dx.doi.org/10.1021/ic1017054 |*Inorg. Chem.* 2011, 50, 2754–2763

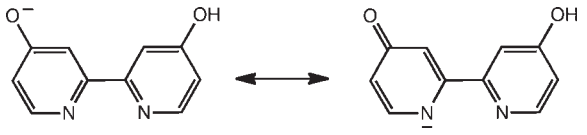

Figure 8. Resonance structures of the monodeprotonated bpy(OH)-(O^{-n}) ligand.

Table 4. Electronic Transition Assignments for $[Ru(bpy)_2(bpy(OH)_2)]^{2+}$ in Water[a]

complex	energy (eV)	λ (nm)	oscillator strength	transition type
protonated	2.968	418	0.129	ML_1CT
	3.050	407	0.131	$ML_{12}CT$
	3.667	338	0.007	ML_1CT
	3.760	330	0.013	ML_1CT
	3.830	324	0.015	ML_1CT
monodeprotonated	2.729	455	0.096	$(ML_{O^-})L_1CT$
	2.897	428	0.078	$(ML_{O^-})L_1CT$
	3.057	406	0.023	$(ML_{O^-})L_1CT$
	3.247	382	0.019	$(ML_{O^-})L_1CT$
	3.360	369	0.041	$(ML_{O^-})L_1CT$
deprotonated	2.516	493	0.057	ML_1CT
	2.683	463	0.030	ML_1CT
	2.912	426	0.025	$(ML_2)L_1CT$
	2.944	422	0.020	$(ML_2)L_1CT$
	3.095	401	0.027	$(ML_2)L_1CT$
	3.127	397	0.012	$(ML_2)L_1CT$
	3.223	385	0.043	$(ML_2)L_1CT$

[a] L_1 = bpy ligand, L_2 = $bpy(OH)_2$ ligand, (ML_2) = mixed metal-L_2 orbital, (ML_{O^-}) = mixed metal-deprotonated pyridine of L_2 ligand.

the tetrabutylammonium hydroxide in the solvent. All of the monodeprotonated complex absorbance band energies occur between that of the fully protonated and fully deprotonated complex. The results are in contrast to studies performed in water where the monodeprotonated form has a similar absorbance spectrum compared to the fully protonated complex, Figure 6. The lack of a shift upon a single deprotonation could be due to a significant degree of hydrogen bonding in water, possibly limiting the increased degree of π-donation from the ligand.

Computational Analysis of Electronic Transitions. Computational studies were utilized to map out the charge transfer transitions above 300 nm for the protonated form of $[Ru(bpy)_2(bpy(OH)_2)]^{2+}$ in both water and 1,2-dichloroethane, Table 4 and Table 5. The lowest energy MLCT transition in $[Ru(bpy)_2(bpy(OH)_2)]^{2+}$ is observed at 418 nm in both solvents and is calculated to be at higher energy than actually observed in experimental data. This trend has also been observed in computational models for the lowest MLCT band in other ruthenium polypyridyl complexes.[43] The transition at 418 nm corresponds to MLCT excitation from a d orbital to the π^* orbital on the nonhydroxylated bpy ligands. There is another calculated transition at slightly higher energy (407 nm in water) with similar oscillator strength to the 418 nm transition. This transition appears as a mixing of two types of MLCT excitations, one to a π^* orbital on the nonhydroxylated bpy ligand and the other to a π^* orbital on the $bpy(OH)_2$ ligand. There are three

Table 5. Electronic Transition Assignments for $[Ru(bpy)_2(bpy(OH)_2)]^{2+}$ in DCE[a]

complex	energy (eV)	λ (nm)	oscillator strength	transition type
protonated	2.966	418	0.137	ML_1CT
	3.046	408	0.139	$ML_{12}CT$
	3.669	338	0.008	ML_1CT
	3.762	330	0.014	ML_1CT
	3.831	324	0.016	ML_1CT
monodeprotonated	2.706	459	0.100	ML_1CT
	2.857	434	0.062	$(ML_{O^-})L_{OH}CT$
	2.939	422	0.018	ML_1CT
	2.980	417	0.036	$(ML_{O^-})L_{OH}CT$
	3.289	377	0.045	$(ML_{O^-})L_1CT$
deprotonated	2.469	503	0.052	ML_1CT
	2.624	473	0.026	ML_1CT
	2.800	443	0.016	$(ML_2)L_1CT$
	2.843	437	0.032	$(ML_2)L_1CT$
	2.987	416	0.016	$(ML_2)L_1CT$
	3.018	411	0.018	$(ML_2)L_1CT$
	3.108	399	0.046	$(ML_2)L_1CT$
	3.204	387	0.017	$(ML_2)L_1CT$
	3.241	385	0.021	$(ML_2)L_1CT$

[a] DCE = 1,2-dichloroethane, L_1 = bpy ligand, L_2 = $bpy(OH)_2$ ligand, (ML_2) = mixed metal-L_2 orbital, (ML_{O^-}) = mixed metal-deprotonated pyridine of L_2 ligand, L_{OH} = protonated pyridine of L_2 ligand.

additional MLCT bands predicted at 324, 330, and 338 nm in water that correspond to MLCT transitions. These bands are also predicted in 1,2-dichloroethane without energy shifts. Experimentally, the bands only shift on the order of a few nanometers and are all highly overlapped.

Computational studies indicate a significantly more complicated absorption manifold in the region above 300 nm upon deprotonation of $[Ru(bpy)_2(bpy(OH)_2)]^{2+}$ in both water and 1,2-dichloroethane, Table 4 and Table 5. None of the individual transitions are as intense as the MLCT transitions observed in the protonated form. In both solvents, the two lowest energy transitions are MLCT from an unmixed metal d orbital to π^* orbitals on the unmodified bipyridine ligands. Computationally, these transitions occur at lower energy (503 and 473 nm) in 1, 2-dichloroethane than in water (493 and 463 nm), a trend consistent with the experimental results. The remaining higher energy transitions studied have been identified as charge transfer excitations from metal d orbitals that significantly mix with orbitals on the deprotonated $bpy(O^-)_2$ ligand into orbitals on the nonhydroxylated bpy ligands. These transitions are effectively Metal−Ligand to Ligand Charge Transfer (MLLCT) transitions. The increased π-donation upon deprotonation (predicted by the resonance structures in Figure 3) results in the formation of new molecular orbitals that are hybrids of the metal d orbitals and the ligand π orbitals on the oxy-substituted bipyridine. As a result, there are numerous overlapping MLLCT bands that cannot be distinguished from each other in the experimental UV/Visible spectrum.

Studies carried out on the monodeprotonated complex using both water and 1,2-dichloroethane confirm the predicted behavior of the $bpy(OH)(O^-)$ ligand, Figure 8. That is, the deprotonated half of the substituted bipyridine ligand forms new hybrid

dx.doi.org/10.1021/ic1017054 |*Inorg. Chem.* 2011, 50, 2754–2763

orbitals by mixing with the metal center, Table 4 and Table 5. All of the calculated MLCT transitions involve mixing of the metal with the deprotonated half of the monodeprotonated ligand into the unsubstituted bipyridine ligands. The calculated energies lie intermediate in energy to the protonated and deprotonated forms of the complex, which is not observed in the experimental results in water where there is no shift in energy. We hypothesize that solvent specific interactions, specifically hydrogen bonding play a significant role in the lack of an energy shift in water experimentally, and future computational studies will investigate the role of the solvent in orbital mixing and the effects of electronic transitions. In the nonpolar solvent, 1,2-dichloroethane, the MLCT transition structure is more complex, although the transitions are intermediate in energy to the protonated and deprotonated complex consistent with the experimental results when solvent specific interactions are not taken into account. In addition, all of the transitions are red-shifted in 1,2-dichloroethane compared to water, consistent with the effects of polarity observed in the experimental data. There are two MLCT transitions (459 and 422 nm) occurring from an unmixed metal d orbital to a π^* orbital on the unmodified bipyridine ligands. Three other transitions are also MLCT, and the originating orbital is a mixture of the metal with the deprotonated half of the monodeprotonated ligand as observed in water. Of these three transitions, the two lowest in energy (434 and 417 nm) occur into a π^* orbital on the protonated half of the monodeprotonated ligand while the third transition (377 nm) occurs into a π^* orbital on the unmodified bipyridine ligands.

CONCLUSION

Electron transfer events are often found intricately woven to proton transfers in biological and chemical systems. We are interested in studying simple molecular systems whereby altering the proton content, the change in electronic properties can be readily observed through spectroscopic and computational means. To this end, $[Ru(bpy)_2(bpy(OH)_2)]^{2+}$ has been synthesized and studied for the effects of the protonation state on the complex. The structural, electrochemical, and light-absorbing properties of the complex were studied in detail for both the protonated and the deprotonated form. Computational studies have shed light on a significant degree of mixing between the metal d orbitals and the modified ligand upon deprotonation, a feature that is elucidated in the UV/Visible absorbance spectrum. In a future paper, we will investigate luminescence properties of the $[Ru(bpy)_2(bpy(OH)_2)]^{2+}$ complex through both experimental and computational means. We also intend to investigate the roles of solvent specific interactions computationally.

ASSOCIATED CONTENT

Supporting Information. Infrared spectroscopy, ^1H NMR spectroscopy, UV/Visible spectroscopy, cyclic voltammetry, and crystallographic data in CIF format. Cartesian coordinates for each species and GAMESS input parameters are also included. This material is available free of charge via the Internet at http://pubs.acs.org.

AUTHOR INFORMATION

Corresponding Author
*E-mail: jared.paul@villanova.edu.

ACKNOWLEDGMENT

Acknowledgment is made to the Donors of the American Chemical Society Petroleum Research Fund for partial support of this research. Support from the College of Liberal Arts and Sciences at Villanova University is gratefully acknowledged. The authors would like to thank Thomas J. Meyer and Javier J. Concepcion of the University of North Carolina at Chapel Hill for helpful discussions.

REFERENCES

(1) Qin, L.; Liu, J.; Mills, D. A.; Proshlyakov, D. A.; Hiser, C.; Ferguson-Miller, S. *Biochemistry* **2009**, *48*, 5121.
(2) McEvoy, J. P.; Brudvig, G. W. *Chem. Rev.* **2006**, *106*, 4455.
(3) Meyer, T. J.; Huynh, M. H. V.; Thorp, H. H. *Angew. Chem., Int. Ed.* **2007**, *46*, 5284.
(4) Reece, S. Y.; Nocera, D. G. *Annu. Rev. Biochem.* **2007**, *78*, 673.
(5) Cukier, R. I.; Nocera, D. G. *Annu. Rev. Phys. Chem.* **1998**, *49*, 337.
(6) Hammes-Schiffer, S. *Acc. Chem. Res.* **2001**, *34*, 273.
(7) Hammes-Schiffer, S. *Acc. Chem. Res.* **2009**, *42*, 1881.
(8) Lebeau, E. L.; Binstead, R. A.; Meyer, T. J. *J. Am. Chem. Soc.* **2001**, *123*, 10535.
(9) Mayer, J. M. *Annu. Rev. Phys. Chem.* **2004**, *55*, 363.
(10) Stubbe, J.; Nocera, D. G.; Yee, C. S.; Chang, M. C. Y. *Chem. Rev.* **2003**, *103*, 2167.
(11) Huynh, M. H. V.; Meyer, T. J. *Chem. Rev.* **2007**, *107*, 5004.
(12) Gagliardi, C. J.; Westlake, B. C.; Kent, C. A.; Paul, J. J.; Papanikolas, J. M.; Meyer, T. J. *Coord. Chem. Rev.* **2010**, *254*, 2459.
(13) Sjodin, M.; Styring, S.; Akermark, B.; Sun, L.; Hammarstrom, L. *J. Am. Chem. Soc.* **2000**, *122*, 3932.
(14) Sjodin, M.; Styring, S.; Wolpher, H.; Xu, Y.; Sun, L.; Hammarstrom, L. *J. Am. Chem. Soc.* **2005**, *127*, 3855.
(15) Irebo, T.; Reece, S. Y.; Sjodin, M.; Nocera, D. G.; Hammarstrom, L. *J. Am. Chem. Soc.* **2007**, *129*, 15462.
(16) Das, A.; McCleverty, J. A.; Ward, M. D.; Jones, C. J.; Thompson, A. M. W. C. *Polyhedron* **1992**, *11*, 2119.
(17) Fecenko, C. J.; Meyer, T. J.; Thorp, H. H. *J. Am. Chem. Soc.* **2006**, *128*, 11020.
(18) Fecenko, C. J.; Thorp, H. H.; Meyer, T. J. *J. Am. Chem. Soc.* **2007**, *129*, 15098.
(19) Himeda, Y.; Onozawa-Komatsuzaki, N.; Miyazawa, S.; Sugihara, H.; Hirose, T.; Kasuga, K. *Chem.—Eur. J.* **2008**, *14*, 11076.
(20) Himeda, Y. *Eur. J. Inorg. Chem.* **2007**, 3927.
(21) Giordano, P. J.; Bock, C. R.; Wrighton, M. S. *J. Am. Chem. Soc.* **1978**, *100*, 6960.
(22) Price, J. M.; Xu, W.; Demas, J. N.; DeGraff, B. A. *Anal. Chem.* **1998**, *70*, 265.
(23) Thompson, A. M. W. C.; Jeffery, J. C.; Liard, D. J.; Ward, M. D. *J. Chem. Soc., Dalton Trans.* **1996**, 879.
(24) Thompson, A. M. W. C.; Smailes, M. C. C.; Jeffery, J. C.; Ward, M. D. *J. Chem. Soc., Dalton Trans.* **1997**, 737.
(25) Crabtree, R. H. *Science* **2010**, *330*, 455.
(26) Hashiguchi, B. G.; Young, K. J. H.; Yousufuddin, M.; Goddard, W. A., III; Periana, R. A. *J. Am. Chem. Soc.* **2010**, *132*, 12542.
(27) Jakubikova, E.; Chen, W.; Dattelbaum, D. M.; Rein, F. N.; Rocha, R. C.; Martin, R. L.; Batista, E. R. *Inorg. Chem.* **2009**, *48*, 10720.
(28) Ji, Z.; Huang, S. D.; Gaudalupe, A. R. *Inorg. Chim. Acta* **2000**, *305*, 127.
(29) Hong, Y.-R.; Gorman, C. B. *J. Org. Chem.* **2003**, *68*, 9019.
(30) Broomhead, J. A.; Young, C. G. *Inorg. Synth.* **1982**, *21*, 127.
(31) Connelly, N. G.; Geiger, W. E. *Chem. Rev.* **1996**, *96*, 877.
(32) Schmidt, M. W.; Baldridge, K. K.; Boatz, J. A.; Elbert, S. T.; Gordon, M. S.; Jensen, J. H.; Koseki, S.; Matsunaga, N.; Nguyen, K. A.; Su, S. J.; Windus, T. L.; Dupuis, M.; Montgomery, J. A. *J. Comput. Chem.* **1993**, *14*, 1347.
(33) Sakai, Y.; Miyoshi, E.; Klobukowski, M.; Huzinaga, S. *J. Comput. Chem.* **1987**, *8*, 256.

(34) Lovallo, C. C.; Klobukowski, M. *J. Comput. Chem.* **2004**, *25*, 1206.
(35) Rillema, D. P.; Jones, D. S. *J. Chem. Soc., Chem. Commun.* **1979**, 849.
(36) Hansen, L. E.; Glowacki, E. R.; Arnold, D. L.; Brernt, G. J.; Chi, B.; Fites, R. J.; Freeburg, R. A.; Rothschild, R. F. N.; Krieg, M. C.; Howard, W. A.; Tanski, J. M. *Inorg. Chim. Acta* **2003**, *348*, 91.
(37) Zakeeruddin, S. M.; Fraser, D. M.; Nazeeruddin, M.-K.; Gratzel, M. *J. Electroanal. Chem.* **1992**, *337*, 253.
(38) Harriman, A. *J. Phys. Chem.* **1987**, *91*, 6102.
(39) Roundhill, D. M. *Photochemistry and Photophysics of Metal Complexes*; Plenum Press: New York, 1994.
(40) Rillema, D. P.; Allen, G.; Meyer, T. J.; Conrad, D. *Inorg. Chem.* **1983**, *22*, 1617.
(41) Daul, C.; Baerends, E. J.; Vernooijs, P. *Inorg. Chem.* **1994**, *33*, 3538.
(42) Kober, E. M.; Sullivan, B. P.; Meyer, T. J. *Inorg. Chem.* **1984**, *23*, 2098.
(43) Rensmo, H.; Lunell, S.; Siegbahn, H. *J. Photochem. Photobiol. A: Chem.* **1998**, *114*, 117.